1522 *Biochemistry* **2010,** *49,* 1522–1532
DOI: 10.1021/bi901748h

BIOCHEMISTRY
including biophysical chemistry & molecular biology
Article

Structure of the Preamyloid Dimer of β-2-Microglobulin from Covalent Labeling and Mass Spectrometry†

Vanessa Leah Mendoza, Kwasi Antwi, Mario A. Barón-Rodríguez,‡ Cristian Blanco,‡ and Richard W. Vachet*

Department of Chemistry, University of Massachusetts, Amherst, Massachusetts 01003. ‡*Present address: Department of Chemistry, Universidad Industrial de Santander, AA 678 Bucaramanga, Colombia.*

Received October 10, 2009; Revised Manuscript Received January 19, 2010

ABSTRACT: β-2-Microglobulin (β2m) self-associates into fibrillar amyloid deposits in the musculoskeletal system of patients undergoing hemodialysis treatment. Previous studies have shown that stoichiometric amounts of Cu(II) at near physiological conditions can cause β2m to organize into native-like dimers prior to forming amyloid fibrils. Here, we report the results from selective covalent labeling reactions combined with mass spectrometry that provide insight into the amino acid residues that mediate dimer formation in the wild-type protein. Using three complementary covalent labeling reagents, we find that the dimer interface is formed by the antiparallel stacking of ABED β-sheets from two β2m monomers. In addition, our data clearly indicate that a dimer interface involving the interactions of D−D strands from separate protein units as seen in the recent crystal structures of two mutant β2m oligomers is unlikely.

β-2-Microglobulin (β2m)[1] is the noncovalently bound light chain of the class I major histocompatibility complex (MHC-I) (*1*). It is a monomeric protein with 99 residues (~12 kDa). It adopts a seven-stranded β-sandwich fold with one β-sheet formed by four strands and the other by three strands. A disulfide bond between Cys25 and Cys80 links strands of the two sheets in the folded state of the protein. β2m is vital for the correct folding, assembly, and cell-surface expression of the MHC-I complex. As part of normal cell turnover, β2m is released from the MHC-I complex and carried to the kidney where it is degraded. Upon renal failure, serum levels of β2m increase up to ~60 times above the normal level of 0.1 μM, and the protein aggregates into insoluble amyloid fibrils in the joints (*2*, *3*). Elevated β2m concentrations alone, however, are not sufficient to trigger fibrillogenesis (*4*, *5*). β2m amyloid formation must therefore result from features unique to hemodialysis, but the exact cause *in vivo* is not known. β2m amyloid fibrils can be generated *in vitro*, though, under acidic conditions (pH < 3.6) (*6*), by removing the first six N-terminal amino acids (*7*), by mixing the protein with collagen at pH = 6.4 (*8*), by sonicating the protein in the presence of sodium dodecyl sulfate at pH = 7.0 (*9*), and by incubating the protein at physiological conditions in the presence of stoichiometric amounts of Cu(II) (*10*, *11*).

Cu(II) as the initiating agent is appealing for a number of reasons. Because several proteins can form amyloid fibrils in the presence of Cu(II) (*12*−*16*), the interactions of this metal with proteins may represent one of the general ways in which amyloid formation can be stimulated. It has been argued that Cu(II) could be the initiating factor for β2m *in vivo* because of the elevated Cu concentrations in dialysate (*10*). The conditions necessary to stimulate β2m fibril formation in the presence of Cu(II) are also arguably more similar to physiological conditions than other methods used to stimulate β2m fibril formation *in vitro*. In addition, a recent *in vitro* study suggests a catalytic role for Cu(II) in β2m fibril formation (*17*), which is important because systemic increases in Cu(II) concentrations are therefore not necessary. While a role for Cu(II) *in vivo* has not been confirmed, addition of the metal is a discrete way to trigger amyloid formation so that the intermediates that precede the fibrils can be more easily studied.

In this study, we use Cu(II) as a trigger to initiate β2m amyloid formation and then study the structure of the dimer, which is the first preamyloid oligomer formed (*17*, *18*). Previous work has shown that incubation of β2m with Cu(II) under near physiological conditions results in the formation of dimers in the first 30 min with tetramers and hexamers not forming for >12−24 h (*17*, *18*). Because the dimer is an intermediate and is always present as a mixture with the monomer and eventually other higher order oligomers, obtaining residue-specific information about the dimer is very challenging by traditional approaches. One recently used approach to solve this problem has been to construct β2m mutants that are capable of crystallizing as oligomers (*19*, *20*). In this way, it has been found that the P32A mutant of β2m forms a dimer in the absence of Cu and the H13F mutant forms a stable hexamer in the presence of Cu. These crystal structures have then been used to support hypotheses about the structural changes necessary for β2m oligomer and amyloid formation. While these crystal structures provide high-resolution atomic-level information, they cannot provide a complete picture of β2m oligomer structure. The β2m mutants do not form fibrils, and so the crystallized oligomers unlike the wild-type oligomers contain structural features that prevent further aggregation. Moreover, it is possible that the selected mutations initiate the formation of oligomers that differ completely from the ones formed by the wild-type protein.

As a complementary approach to these crystallographic studies, we describe here the use of covalent labeling along with mass spectrometry (MS) to gather insight into the structure of the

†This work was supported by the National Institutes of Health (R01 GM075092).

*Corresponding author. E-mail: rwvachet@chem.umass.edu. Telephone: (413) 545-2733. Fax: (413) 545-4490.

 Published on Web 01/20/2010

wild-type β2m dimer. This method relies on amino acid specific reactions of solvent-exposed amino acid side chains and tandem MS (MS/MS) to identify the modified residues. Covalent labeling combined with MS and MS/MS has been used to map protein surfaces, identify ligand-binding sites, study protein−protein and protein−nucleic acid complexes, and detect ligand-induced conformational changes (*21*). These covalent labeling methods provide information about protein structure and interactions by comparing the reactivity of amino acid side chains in solution under two or more different conditions. MS/MS is then used to identify the specific amino acids that undergo significant changes in reactivity. This approach is well suited for providing insight into the dimeric intermediate of β2m because amino acid side chains are usually buried upon formation of new protein−protein interfaces, and buried amino acids are much less reactive than exposed amino acids. Furthermore, the specificity of MS allows this information to be obtained even under conditions in which a mixture of β2m forms is present.

Using three complementary covalent labels with MS detection, we show that the dimer is formed by the interactions of two four-strand β-sheets from two monomers. Confidence in this assignment arises because our covalent labeling reactions are able to probe about one-third of β2m's surface-exposed amino acids, and these amino acids are evenly spread across the protein. Moreover, almost one-half of the residues at the dimer interface are probed with the covalent labels used in this study. Overall, our results indicate the potential power of covalent labeling and MS for studying oligomer-forming proteins, and they provide specific structural information that could inspire efforts to design inhibitors of β2m oligomerization and fibril formation.

MATERIALS AND METHODS

Materials. Human β2m was obtained from Fitzgerald Industries International, Inc. (Concord, MA). Diethyl pyrocarbonate (DEPC), 2,3-butanedione (BD), sulfo-*N*-hydroxysuccinimide acetate (NHSA), imidazole, dithiothreitol (DTT), copper(II) sulfate (CuSO4), 3-morpholinopropanesulfonic acid (MOPS), potassium acetate, arginine, ubiquitin from bovine erythrocytes, equine heart cytochrome *c*, equine skeletal muscle myoglobin, chicken egg white ovalbumin, human hemoglobin, and bovine transferrin were purchased from Sigma-Aldrich (St. Louis, MO). Tris(hydroxymethyl)aminomethane (Tris) was purchased from EM Science (Gladstone, NJ). Urea was purchased from Mallinckrodt Chemicals (Phillipsburg, NJ). Trypsin was from Promega (Madison, WI), and chymotrypsin was purchased from Roche Diagnostics (Indianapolis, IN). Centricon molecular weight cutoff (MWCO) filters were obtained from Millipore (Burlington, MA). Deionized water was prepared from a Millipore (Burlington, MA) Simplicity 185 water purification system.

Formation of β2m Oligomers and Fibrils. Reports have shown that discrete oligomers precede β2m amyloid fibrils when monomeric β2m is incubated under near physiological conditions in the presence of Cu(II) (*17*, *18*). Amyloid fibrils were formed by incubation of 100 μM β2m in 200 mM potassium acetate, 500 mM urea, and 25 mM MOPS (pH 7.4) with 200 μM copper(II) sulfate at 37 °C. All components were equilibrated at 37 °C prior to Cu(II) addition and immediately returned to 37 °C after mixing. The covalent labels were added to aliquots of incubated β2m taken at several time points after initiating the amyloid fibril formation reaction.

Carbethoxylation with DEPC. Stock solutions of DEPC were prepared in acetonitrile. The DEPC reactions of β2m were performed for 1 min at 37 °C and were initiated by adding 0.25 mM DEPC. The total reaction volume for the experiments was 30 μL, and the total amount of acetonitrile added was ~1.5%. The reactions were quenched after 1 min by adding 10 mM imidazole.

Acetylation with NHSA. Stock solutions of NHSA were prepared in water. The labeling of β2m with 0.30 mM NHSA was carried out for 1 min at 37 °C. The total reaction volume for the experiments was 30 μL. The reactions were quenched by adding 10 mM Tris.

BD Modification. Stock solutions of BD were prepared in water. The reactions of β2m with 35 mM BD were performed in the dark for 1 min at 37 °C. Reactions were carried out in the dark to avoid possible photoactivation of the label, which could enhance nonspecific reactions with residues other than arginine (*22*, *23*). The total reaction volume for the experiments was 30 μL. The reactions were quenched by adding 100 mM arginine.

Proteolytic Digestion. Before proteolytic digestion, all modified samples were purified using a 10000 MWCO filter and reconstituted with deionized water to a final concentration of 300 μM. Purified β2m samples in 25 mM Tris-HCl (pH 7) and 1 mM $CaCl_2$ were first reacted with 10 mM DTT at 37 °C for 45 min to reduce the disulfide bonds. This was followed by addition of acetonitrile and incubation at 37 °C for 45 min. Trypsin and chymotrypsin (1 μg/μL) were then added to DEPC-modified samples to yield a final enzyme/substrate ratio of 1:20. For the NHSA- and BD-modified β2m samples, only chymotrypsin (1 μg/μL) was added. Although trypsin is the most reliable and robust protease, chymotrypsin was used instead because trypsin can no longer cleave proteins after acetylated lysine and modified arginine residues. All samples were digested at 37 °C for 16 h. The enzymes were inactivated by adding 2 μL of acetic acid, and the samples were immediately analyzed.

Desalting. Desalting of the protein samples just prior to electrospray ionization (ESI) mass spectrometry (MS) analyses was performed using a 5 mL HiTrap desalting column from Amersham Biosciences (Piscataway, NJ). The column was first equilibrated with 30 mL of the mobile phase (10 mM ammonium acetate, pH = 7.4) at a flow rate of 5 mL/min. Then, between 100 and 150 μL of incubated sample was injected onto the column via a sample loop attached to a homemade setup. The oligomeric intermediates were eluted at a flow rate of 10 mL/min using 10 mM ammonium acetate (pH = 7.4), which was filled into a syringe and delivered by a syringe pump. The β2m fraction eluting from the column was collected between 20 and 22 s and analyzed immediately by ESI-MS.

Instrumentation. The amount of modification was determined by removing an aliquot of the purified β2m and analyzing the samples using a Bruker Esquire-LC quadrupole ion trap mass spectrometer (Billerica, MA) equipped with an ESI source. The ESI source was operated at a spray voltage of 3.5 kV, and the capillary temperature was set at 300 °C. The voltages for the transfer optics between the ESI source and the ion trap were optimized for maximum signal, with typical skimmer 1 and capillary offset values of 30−35 and 50−60 V, respectively.

The proteolytic fragments were separated by an Agilent HP1100 (Wilmington, DE) HPLC system with a C18 column (15 cm × 2.1 mm, 5 μm particle size; Supelco, St. Louis, MO) for online analysis by MS and MS/MS. The fragments of

NHSA- and BD-modified β2m were eluted using a linear gradient of methanol that increased from 5% to 70% over 20 min and from 70% to 100% over the final 2 min at a flow rate of 0.250 mL/min. For the fragments of DEPC-modified β2m, a linear gradient of methanol that increased from 5% to 70% over 30 min and from 70% to 100% over the final 3 min was used. For both gradient conditions, water comprised the balance of the solvent, and a total of 0.1% acetic acid was present. The LC effluent was fed into the mass spectrometer with similar ESI source conditions as described above. Tandem mass spectra were acquired using collision-induced dissociation (CID) with isolation widths of 1.0 Da and excitation voltages between 0.6 and 1.0 V. Peptide sequences were determined from the MS/MS data via *de novo* sequencing or with the help of BioTools (Bruker Daltonics, Billerica, MA).

Sequencing of β2m to identify the specific amino acids modified by BD is not possible using CID, so electron transfer dissociation (ETD) was used to identify the specific modification sites. In the CID process the BD label is readily lost without any associated information about its location in the sequence. The ETD experiments were carried out using a Bruker HCT ETD II (Billerica, MA) equipped with an ESI source. ETD was performed using a total reaction time of 25 ms and low mass cutoff of 100. Accumulation times for the fluoranthene radical anion, which was used as the ETD reagent, were typically between 3 and 5 ms.

A JMS-700 MStation (JEOL, Tokyo, Japan) double-focusing mass spectrometer equipped with a standard ESI source was used to acquire mass spectra of the β2m oligomers after desalting the incubation solution. The ESI source conditions that were used are the following: desolvating plate temperature, 100 °C; orifice temperature, 140 °C; orifice potential, 60 V; ring lens potential, 100 V. ESI-MS experiments of the desalted protein samples were used to measure the average charge states of these oligomers and to estimate their surface areas using a method described previously by Kaltashov and co-workers (*24*). The spectra were acquired by scanning the magnet at a rate of 5 s/decade.

Amino Acid Modification Percentage. The percent modification of each labeled amino acid was determined by comparing the LC-MS intensities of modified and unmodified proteolytic peptide fragments containing the amino acid of interest. For each peptide fragment, the modified form eluted after the unmodified form with the difference in retention times ranging from 1 to 12 min. The ion intensities of both modified and unmodified peptides were determined from extracted ion chromatograms; as an example, see Figure S1 in the Supporting Information. The reported ion intensities were determined by averaging a 0.4 min time range centered on the given chromatographic peak. The percent modification was then obtained by dividing the ion intensity of the modified fragment (I_{modified}) by the sum of the ion intensities for the modified (I_{modified}) and unmodified ($I_{\text{unmodified}}$) fragments as shown in eq 1. The errors are reported as the standard error of the mean using the data from three separate modification reactions. Because ion intensity ratios were used, day-to-day ion intensity variations, which can be common in mass spectrometers, were minimized, and low modification levels could be accurately determined.

$$\%\ \text{modification} = \frac{I_{\text{modified}}}{I_{\text{modified}} + I_{\text{unmodified}}} \times 100 \qquad (1)$$

Determination of Solvent Accessibility. The 3D structures of β2m that were examined were obtained from the Protein Data Bank: 2D4F for monomeric β2m (*25*), 2F8O for the P32A dimer (*19*), and 3CIQ for the H13F hexamer (*20*). The solvent-accessible surface areas (SASA) of individual amino acid side chains were calculated from the PDB coordinate files using GETAREA (http://curie.utmb.edu/getarea.html) (*26*). For these SASA calculations, a 4.0 Å probe radius was used because the radii of the covalent labels used in this study range from ~3.5 to 4.5 Å. To determine the surface area of the whole protein for comparison with the ESI-MS results, a 1.4 Å probe radius was used.

Docking Calculations. All simulations were performed using the β2m subunit taken from the crystal structure of the human MHC-I complex (PDB ID: 1DUZ) (*27*), which contains 99 amino acid residues. Met0 was eliminated from the original set of coordinates in order to resemble the wild-type protein used in the labeling experiments. Hydrogen atoms were explicitly added to the protein model, and His residues were considered to be neutral, as shown in nuclear magnetic resonance (NMR) studies by Esposito and co-workers (*28*). Water molecules, as a TIP3P model (*29*), were also added until a cubic simulation cell of side length 7.8 nm was achieved.

Five nanosecond molecular dynamics (MD) simulations were performed to determine the most probable conformation of wild-type β2m. The MD simulations were run at 310 K with periodic boundary conditions in an nPT ensemble and with the AMBER94 force field (*30*, *31*) implemented in GROMACS (*32*−*34*). Protein structures were selected every 1 ps, and those structures that had root-mean-squared displacements of the backbone less than 0.05 nm were clustered together. The final structure that was used in the docking calculations was chosen from the largest cluster of structures.

The docking of two wild-type monomeric β2m molecules was performed to evaluate possible dimer interfaces. The docking search optimizes desolvation, grid-based shape complementarity, and electrostatics using a fast Fourier transform algorithm ZDOCK2.3 (*35*, *36*) and provides a score for all possible docked conformations. The structures of the ten top-scoring dimers were then energy-minimized with solvent present using the AMBER94 force field. The adaptive Poisson−Boltzmann solver (*37*) within the AMBER force field was used to evaluate the free energy binding ($\Delta\Delta G$) of each dimer.

RESULTS

All covalent labeling experiments were performed on wild-type protein under solution conditions in which β2m forms amyloid fibrils. In previous studies, dynamic light scattering, size-exclusion chromatography, and MS showed that β2m oligomers are formed sequentially with the dimer first appearing between 30 min and 1 h and the initial form of the tetramer appearing after approximately 12−24 h (*17*). These previous studies also showed that the smaller oligomers are in equilibrium with one another and can therefore dissociate to lower order oligomers or to the monomer. Because complete isolation of the dimer was not possible without some dissociation back to the monomer, the chemical modification reactions were performed at different times before (t = 0 min) and after (t = 2 min, 0.5 h, 1 h, 1.5 h, and 2 h) adding Cu(II) to initiate the amyloid-forming reaction. The dimer percentage at time points after the addition of Cu(II) increases from 0% to 20% based on ESI-MS measurements of the desalted sample under amyloid-forming conditions, as described previously (*17*).

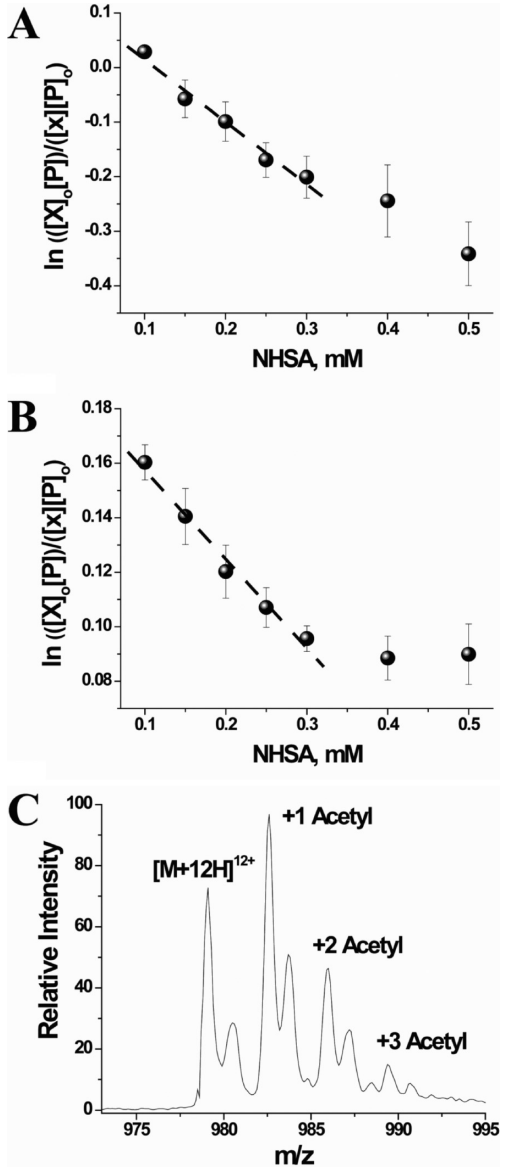

FIGURE 1: (A) Dose−response plot for Lys6 (fragment Thr4−Tyr10) after reaction with NHSA. (B) Dose−response plot for Lys75 (fragment Tyr67−Tyr78) after reaction with NHSA. The plot for each reactive residue is produced from LC-MS data of the proteolytic digests of the modified protein. The $[P]/[P]_o$ ratio is obtained by dividing the peak area for the unmodified fragment by the sum of the peak areas for the modified and unmodified fragments. The difference between the [P] and $[P]_o$ values is used to determine the concentration of NHSA, [X]. (C) Expanded view of the mass spectrum showing the extent of acetylation for the +12 charge of β2m at $t = 0$. The second peak of each doublet is due to a fraction of the protein being oxidized at Met99. This residue is easily oxidized during protein storage. The portion of the protein molecules that are oxidized is typically about 20−30% of the total protein.

Covalent Labeling with NHSA. Amino groups such as the ε-NH_2 of lysine residues and the N-terminal α-NH_2 can react with NHSA. First, the optimum reaction time and molar ratio of NHSA were determined. As described previously (*21*, *48*), plots of the second-order reaction kinetics for the modified peptide fragments can be used to ensure that the covalent label itself does not disrupt the structure of β2m near a particular reactive amino acid residue (Figure 1A,B). For monomeric β2m, deviations from linearity, which are indicators of label-induced structural perturbations, occur at a 4-fold molar excess of NHSA for most of the modified proteolytic peptide fragments. Hence, the label was added to the β2m samples at a 3-fold molar excess to avoid label-induced protein structural changes. Upon modification with a 3-fold excess of NHSA for 1 min at 37 °C, the addition of up to three acetyl groups is reproducibly observed, with the average number of modifications to the whole protein around 1 (Figure 1C).

Identifying the amino acids that are acetylated is necessary to pinpoint the specific residues that become less reactive as the dimer concentration increases, and this identification was achieved by proteolytic digestion and LC-MS/MS analyses. LC-MS/MS analyses indicate that the N-terminus, almost all of the lysines (Lys6, Lys19, Lys41 (and/or Lys48), Lys58, Lys75, Lys91, and Lys94), and Asn83 are labeled to different degrees. The unmodified and modified fragments containing the lysine residues were detectable at all time points; however, the level of modification for some residues changed over time (*vide infra*). The modified peptide Lys41−Leu54, which contains both Lys41 and Lys48, had too low abundance to obtain definitive MS/MS spectra, but this peptide fragment was observed at all time points. We speculate that Lys48 is the modified residue in this peptide as the solvent-accessible surface area (SASA) of this residue in monomeric β2m (from PDB ID: 2D4F) is two times greater than that of Lys41. Modification of an Asn residue, Asn83, is unprecedented as NHSA has only been reported to react with N-terminal amines and lysine residues (*39*), but the tandem mass spectrum of the modified fragment Ala79−Leu87 unambiguously identifies Asn83 as the modified amino acid.

When the covalent labeling reactions with NHSA are performed at different time points after initiating the formation of the dimer, the modification extents of some residues change as the concentration of the dimer increases in solution (Figure 2 and Figure S2 in the Supporting Information). The data in these figures are obtained by measuring the modification percentage, as described in the Materials and Methods (e.g., Figure S1 in the Supporting Information), for the peptide fragments containing the indicated residues. For each time point, the modification reaction was repeated three times. Tables S1 through S18 in the Supporting Information show the raw intensity data for each of the three trials for all of the data points in Figure 2. Figure S3 in the Supporting Information shows examples of how peptide ion intensities change after the dimer becomes more populated in solution. Because the percent modification is determined using the ion intensity ratios of the unmodified and modified peptide fragments, small changes in modification levels can be accurately and precisely determined.

From the data in Figure 2 and Figure S2 in the Supporting Information, we find that the levels of modification of Lys58, Lys75, and Lys94 increase by about 20%, 20%, and 40%, respectively, from before Cu(II) is added to 2 h after Cu(II) is added. In contrast, the reactivity of the N-terminus, Lys6, and Lys91 decreases after addition of Cu(II). The N-terminus has the greatest drop in extent of modification, decreasing 30% immediately upon addition of Cu(II). The reactivity of this residue, however, does not change anymore as the dimer forms in solution. Like the N-terminus, the reactivity of Lys91 initially decreases, about 20%, after addition of Cu(II); however, there is a small 5% increase in the extent of modification from 2 min to 2 h as the dimer's concentration increases in solution. Lys6 behaves differently than the N-terminus and Lys91 in that its reactivity does not drop immediately upon addition of Cu(II) but instead decreases as the dimer's concentration increases (Figure 2A). The

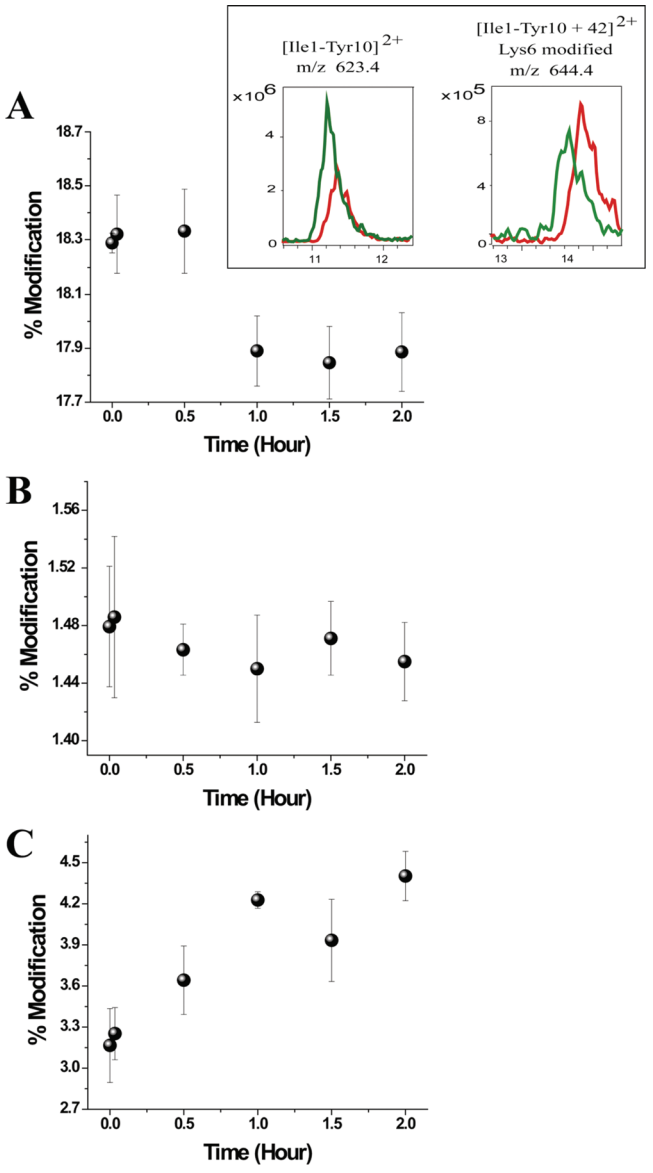

FIGURE 2: Extent of NHSA modification for selected residues, (A) Lys6, (B) Asn83, and (C) Lys94, throughout the course of the dimer formation reaction. The inset in (A) shows the extracted ion chromatograms of the unmodified (m/z 623.4) and Lys6-modified (m/z 644.4) forms of the fragment Ile1−Tyr10 in the absence of Cu(II) (red trace) and 2 h after addition of Cu(II) (green trace). The ion intensities of the unmodified and modified peptide ions were determined from these chromatograms. Ion intensity changes in the absence (red trace) and presence (green trace) of Cu(II) show the decrease in the extent of modification of Lys6 when β2m interacts with Cu(II). The percent modification was obtained using the ratiometric approach shown in eq 1.

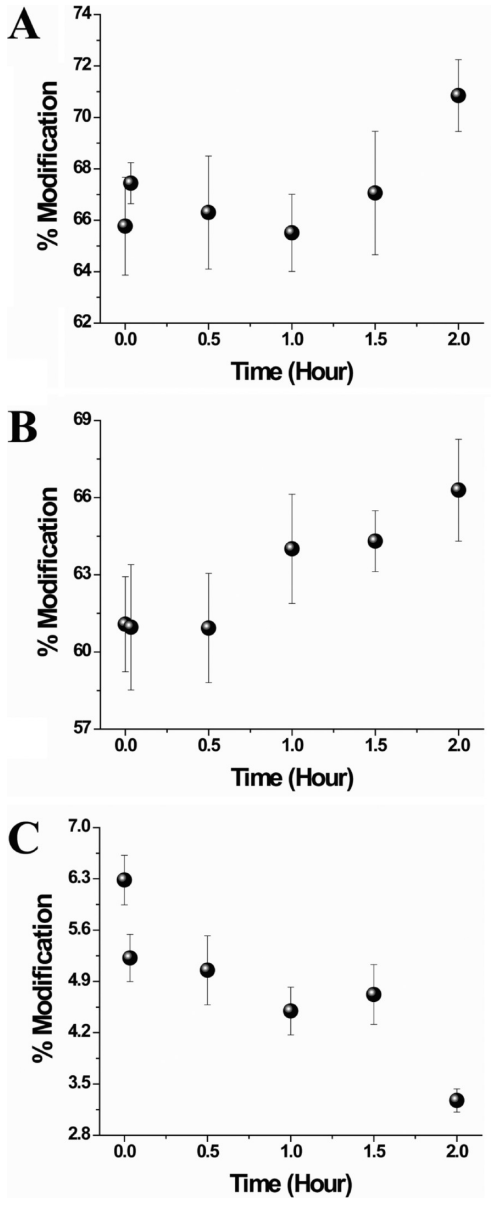

FIGURE 3: Extent of DEPC modification for selected residues, (A) Ser88, (B) His51, and (C) Tyr63, throughout the course of the dimer formation reaction.

reactivity of Lys19, Lys41/48, and Asn83 remains approximately constant up to 2 h after the addition of Cu(II).

In summary, the NHSA reactivity data indicate that of the nine modified residues in β2m four of them undergo a notable change in reactivity as the dimer is formed in solution. The modification extents of Lys58, Lys75, and Lys94 increase, whereas the reactivity of Lys6 decreases. The N-terminus and Lys91 also decrease in reactivity, but their lower reactivity appears to be mostly due to Cu binding rather than the formation of dimer.

Covalent Labeling with DEPC. DEPC reacts readily with histidine residues but can also react with amine and hydroxyl groups at neutral pH. The DEPC experiments were performed in much the same way as the lysine acetylation studies. Based on second-order kinetic plots of each modified peptide, a 2.5-fold molar excess of DEPC was used to minimize DEPC-induced β2m structural changes (Figure S4 in the Supporting Information). As was the case with the NHSA reactions, the reaction time was kept short (1 min) to avoid dimer dissociation or monomer association and to minimize DEPC hydrolysis by water. Under the experimental conditions used, the addition of up to three carbethoxy groups was observed to the whole protein, and the average number of modifications was between 1 and 2. Proteolytic digestion of the protein and LC-MS/MS analyses indicate that DEPC reacted with the N-terminus, Thr4, His13, Lys19, Tyr26, Ser28, His31, Ser33, His51, Ser57/Lys58, Tyr63, Tyr67, Lys75, Ser88, and Lys94. These modifications were observed at all time points, but the level of modification for some residues changed over time (*vide infra*). In all cases but one (Ser57/Lys58), the specific amino acids that were modified could be determined unambiguously from the MS/MS data.

The reactions with DEPC reveal that some residues change in reactivity as the dimer's concentration increases in solution (Figure 3 and Figure S5 in the Supporting Information; the raw intensity data for the residues shown in Figure 3 are included in Tables S19 through S36 in the Supporting Information). LC-MS data reveal that the percent modifications of six residues increase upon dimer formation. These residues are Thr4, His51, Ser57/Lys58, Lys75, and Lys94. Thr4 undergoes the least significant change in reactivity, with about a 3% increase when about 20% dimer is present. His51 and either Ser57 or Lys58 increase in reactivity by about 10%. The increased reactivity of Ser57 or Lys58 is consistent with the increased reactivity of Lys58 in the NHSA experiments described above. The reactivity of Lys75 and Lys94 increases the most, 25% and 30%, respectively, as the dimer's concentration increases. The significantly increased reactivities of Lys75 and Lys94 agree with the NHSA data described above. Finally, the reactivity trend of Ser88 is somewhat unclear. For all but the last time point (2 h), this residue reacts with DEPC in a fairly constant manner.

The modification extents of nine amino acids drop after Cu is added, but only five of these residues show decreased reactivity as the dimer's concentration increases. The reactivities of the N-terminus, His31, Ser33, and Tyr67 drop upon Cu(II) binding but change little or none as the dimer forms. His13, Lys19, Tyr26, Ser28, and Tyr63, however, do decrease in reactivity as more and more dimer is formed.

The results from the DEPC reactions are consistent with the NHSA experiments, except for the reactivity trend of Lys19. In contrast to the constant modification of fragment Ser11−Phe22 with NHSA during the course of the dimer-forming reaction, this fragment showed a 10% decrease in modification of Lys19 with DEPC over time (Figure 3). This slight discrepancy might be due the microenvironment around Lys19, which could influence the reactivity of the two differently charged labels to an unequal extent.

In summary, our results indicate that the reactivities of DEPC with His13, Lys19, Tyr26, Ser28, and Tyr63 decrease as the dimer is formed, whereas the reactivities of Thr4, His51, Ser57/Lys58, Lys75, and Lys94 increase as the dimer is formed. The modification extents for the N-terminus, His31, Ser33, and Tyr67 also decrease, but their lower reactivity appears to be due to Cu binding rather than the formation of dimer.

Covalent Labeling with Butanedione. Unlike DEPC, which reacts with many nucleophilic groups, BD reacts specifically with arginine. The reaction is reversible at pH <9, so higher reagent doses are necessary to improve the product yield. The excess reagent allows pseudo-first-order kinetic plots to be used to ensure the structural integrity of the protein (Figure S6 in the Supporting Information). Based on these plots, a reagent excess of 350 was chosen. Under these reaction conditions, up to two modifications were detected with an average number of modification of less than 1. The LC/MS and ETD data indicate that BD reacts with Arg3, Arg12, Arg45, and Arg97 but not Arg81.

The reactions of BD with β2m reveal that each of the four reacting arginine residues undergoes changes in reactivity after the addition of Cu(II) (Figure S7 in the Supporting Information). The reactivities of Arg3 and Arg97 dramatically increase (about 80%) immediately after Cu(II) is added but do not change much as the dimer's concentration increases. The reactivity trends of Arg12 and Arg45, however, do change as the dimer is formed. The modification extent of Arg12 decreases over time, whereas the modification extent of Arg45 gradually increases.

Table 1: Summary of Percentage Changes for Modified Amino Acids from $t = 0$ to $t = 2$ h after Adding Cu(II)

residue	$t = 0$	$t = 2$ h	% change
NHSA			
N-terminus	84 ± 3	60.7 ± 0.3	28
Lys6	18.31 ± 0.04	17.9 ± 0.1	2
Lys19	7.1 ± 0.2	7.2 ± 0.2	
Lys41/Lys48	13.2 ± 0.7	13.2 ± 0.8	
Lys58	16.1 ± 0.7	19.0 ± 0.1	18
Lys75	1.37 ± 0.07	1.62 ± 0.08	18
Asn83	1.48 ± 0.04	1.46 ± 0.03	
Lys91	27 ± 1	24.0 ± 0.4	11
Lys94	3.2 ± 0.3	4.4 ± 0.2	38
DEPC			
N-terminus	99 ± 3	68.1 ± 0.6	31
Thr4	86.5 ± 0.7	89.5 ± 0.6	3
His13	45 ± 1	40.0 ± 0.7	11
Lys19	13.0 ± 0.9	11.5 ± 0.6	12
Ty26	0.74 ± 0.06	0.45 ± 0.06	39
Ser28	0.24 ± 0.01	0.11 ± 0.01	54
His31	1.6 ± 0.2	0.8 ± 0.2	50
Ser33	1.74 ± 0.06	1.19 ± 0.06	32
His51	61 ± 2	66 ± 2	8
Ser57/Lys58	39 ± 2	47 ± 2	21
Tyr63	6.3 ± 0.3	3.3 ± 0.2	48
Tyr67	2.2 ± 0.2	1.5 ± 0.1	32
Lys75	0.31 ± 0.04	0.38 ± 0.02	23
Ser88	66 ± 2	72 ± 1	9
Lys94	28 ± 2	36 ± 2	29
BD			
Arg3	0.5 ± 0.2	1.01 ± 0.04	100
Arg12	1.3 ± 0.1	0.64 ± 0.06	51
Arg45	3.8 ± 0.3	6.5 ± 0.5	71
Arg97	2.7 ± 0.5	4.9 ± 0.2	81

Table 2: Proteins Used To Generate the Charge−Surface Area Calibration Plot

protein	PDB ID	surface area (Å^2)	average charge
ubiquitin	1UBQ	4758	5.5
cytochrome *c*	1HRC	6232	7.3
myoglobin	1WLA	8017	8.2
ovalbumin	1OVA	15586	14.2
hemoglobin	1A3N	24548	17.3
transferrin	1JNF	27395	18.5

A summary of the percentage changes for each of the modified amino acids monitored at $t = 0$ and $t = 2$ h is shown in Table 1.

Determination of Surface Area of β2m Oligomers. ESI-MS experiments were performed to measure the average charge states of β2m oligomers and estimate their surface areas from these measurements using a method recently described by Kaltashov and co-workers (*24*). That group recently demonstrated that the average charge state of a protein in its ESI mass spectrum is related to its surface area. Using mass spectral data for six proteins with known surface areas (Table 2), we generated a calibration curve by plotting the natural log of the measured average charge state as a function of the natural log of the protein surface area (Figure 4A). The resulting plot has a slope of 0.68 ± 0.02, which compares favorably with the theoretically expected slope of 0.75 and a slope of 0.69 ± 0.02 measured by Kaltashov and co-workers (*24*). To obtain the average charge state of each protein, a Gaussian fit of relative abundance of each charge state

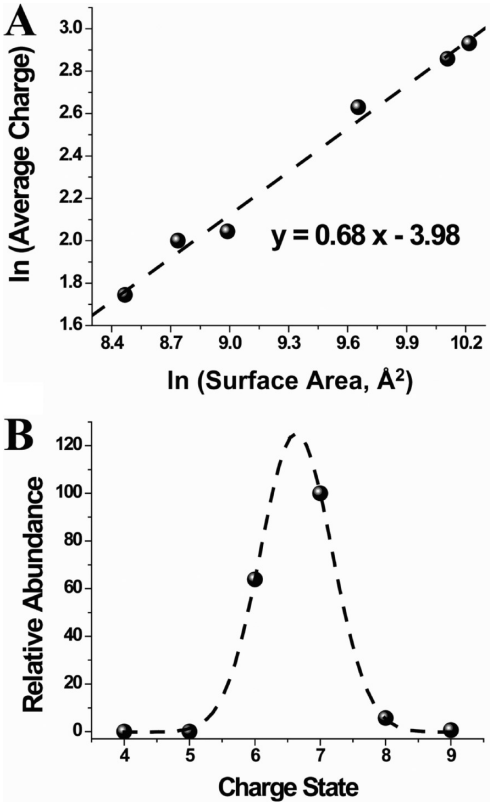

FIGURE 4: (A) Calibration plot obtained from mass spectra of the proteins in Table 2, which is used to measure the surface areas of the β2m oligomers. (B) A plot of ion intensity as a function of charge state for the β2m dimer. A Gaussian fit is used to determine the average charge state.

Table 3: Measured Surface Areas of β2m Oligomers

	measured surface area (Å^2)			
days of incubation	monomer	dimer	tetramer	hexamer
0	6515	11586		
1	6743	11546	21248	
3	6655	11435	20843	25050
5	6660	11370	21110	24982
7	6393	11211	21228	24837

for the protein in the mass spectrum versus the measured charge states was used (Figure 4B).

This approach for estimating oligomer surface area was used at different points after adding Cu(II) to initiate the amyloid-forming reaction. The average charge states of the monomer and oligomers of β2m ions were determined from ESI mass spectra like that shown in Figure S8 in the Supporting Information, and these values were used to estimate their surface areas (Table 3). The estimated surface areas of the monomer, dimer, tetramer, and hexamer are 6590 ± 140, 11430 ± 150, 21110 ± 190, and 24960 ± 110 Å^2, respectively.

DISCUSSION

The goal of the current study is to obtain structural information about the β2m dimer that is formed after the protein binds Cu and before it proceeds to form amyloid fibrils. Our group and others have shown that β2m forms dimers, tetramers, and hexamers (*17*, *18*). Because no odd-numbered oligomers are observed, the dimer is likely the basic unit of the tetramer and hexamer. Hence, characterizing the dimeric intermediate will not only help to delineate the early steps of β2m fibrillogenesis but will also aid in determining the structures of the tetramer and hexamer.

Our approach in this work has been to use covalent labeling along with MS detection because of the utility of this method for studying protein−protein interactions in solution. Two mutant β2m oligomer crystal structures are available (*19*, *20*), and these structures provide convenient high-resolution information to which our data can be compared. These crystal structures, however, are not of the wild-type protein, and the specific mutations in each case prevent the protein from forming amyloid fibrils. This fact means that our labeling experiments provide more relevant information about the structural changes necessary for wild-type β2m to form amyloid-competent oligomers.

Several factors affect the covalent labeling efficiency of amino acid side chains, but solvent accessibility is the most important (*21*). Consequently, covalent labeling is especially effective at identifying residues that mediate protein−protein interactions because the solvent accessibilities of such residues typically undergo noticeable changes. In the case of β2m, complete isolation of the dimer is not possible without some dissociation back to the monomer, so the covalent labeling experiments had to be performed at different times after adding Cu(II) to initiate the amyloid-forming reaction. Our previous work has shown that an appreciable amount of dimer is formed within 30 min and no tetramer is formed until after 12 h. Thus, by monitoring the modification extents of different residues for the first 2 h after the addition of Cu, we can obtain some insight into the residues that undergo changes in solvent accessibility over time, suggesting that they are important for mediating dimer formation. The β2m residues that react with NHSA, DEPC, and BD are widely distributed along the polypeptide chain and on the surface of the protein. Thus, we cover most regions of the protein. The structural data obtained covers 25 of the protein's 99 residues and ~30% of the surface-exposed residues (Figure 5).

Most of the amino acids probed by the covalent labels undergo a change in reactivity after Cu(II) is added, but we will focus our discussion on those amino acids that undergo changes as the dimer forms in solution. Of the 25 modified residues, only three amino acids, Lys41 (and/or Lys48), Asn83, and Ser88, have no significant change in reactivity after Cu(II) is added and the amyloid-forming reaction has proceeded for 2 h. No change in reactivity suggests that these residues retain a similar chemical environment upon Cu binding and dimer formation. The residues that undergo a change in reactivity upon Cu(II) binding, but change little or none as the dimer forms, are the N-terminus, Arg3, His31, Ser33, Tyr67, Lys91, and Arg97. The changes in reactivity associated with these residues are important because they provide some insight into the structural changes caused by Cu binding that enable the protein to dimerize; however, the focus of this work is the identification of the amino acids that are involved in mediating the interactions between protein units in the dimer. The remaining 14 residues, including Thr4, Lys6, Arg12, His13, Lys19, Tyr26, Ser28, Arg45, His51, Lys58 (and/or Ser57), Tyr63, Lys75, and Lys94, undergo changes in their labeling extent as the dimer's concentration increases in solution. Because solvent accessibility is the key factor controlling the relative reactivity of these residues, the protection from modification of some of these residues in the dimer suggests that these

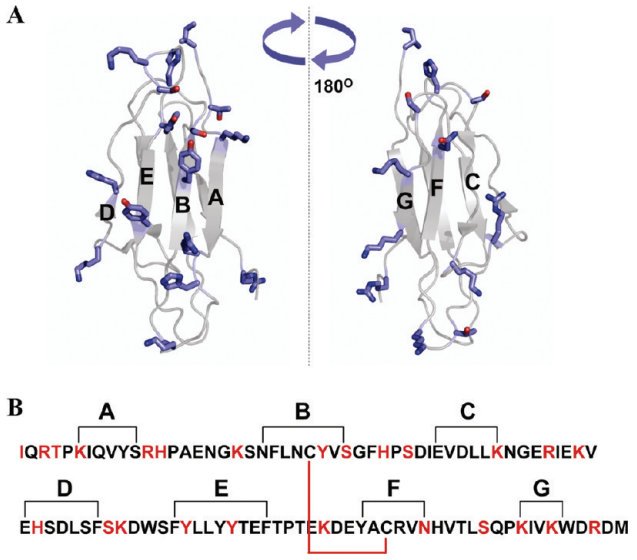

FIGURE 5: (A) Ribbon representation of monomeric β2m (PDB ID: 2D4F). Amino acids modified by the covalent labels are shown as sticks. (B) Amino acid sequence of β2m showing strand nomenclature (*40*). Black lines show amino acids on each β-strand. The internal disulfide bond is shown in red. The amino acids probed by the covalent labels are shown in red.

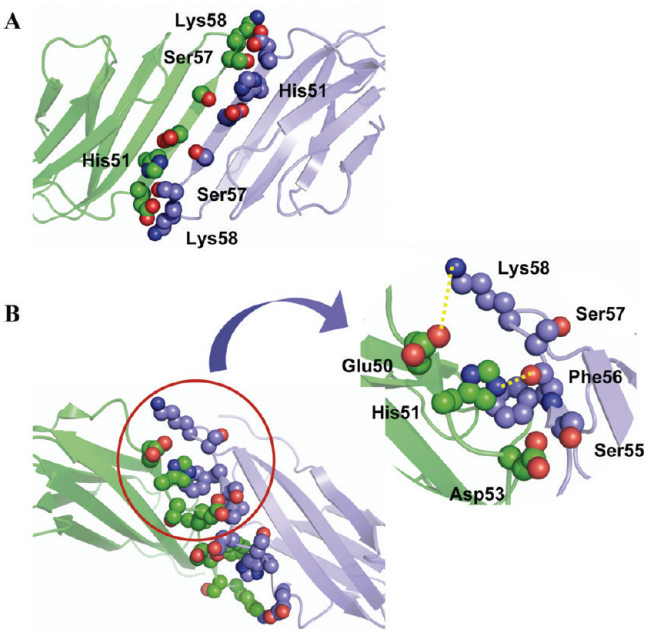

FIGURE 6: Dimers formed by D−D strand interactions. Amino acids Glu50−Lys58 are shown as spheres. (A) D−D strand interface of the crystallographic dimer of P32A. (B) Interaction of adjacent D strands in one of the dimer units (AB chains) in the H13F hexamer. Interstrand interactions of the side chains of Glu50 and His51 of one monomer with the side chain of Lys58 and the backbone of Phe56, respectively, of another monomer are shown.

residues are at or near the dimer interface and implies that they may perhaps contribute to the stability of the dimer.

Previous reports showed that the β2m oligomers are native-like in structure (*41*), so the known structure of the Cu-free monomer is a useful reference point for interpreting our data. In addition, the recent crystal structures of two mutant β2m oligomers, the P32A dimer (PDB ID: 2F8O) (*19*) and the H13F hexamer (PDB ID: 3CIQ) (*20*), also provide a very useful basis for comparison to our data. The symmetry of the H13F hexamer is such that each protein unit interfaces with two other protein units in distinct ways. Thus, together the P32A dimer and the H13F hexamer provide three dimer interfaces to which we can compare our data. The overall fold of β2m changes little in these mutant oligomers, which is consistent with the expected native-like structure of the wild-type oligomers. Upon comparing our data with the mutant oligomers and the wild-type monomer, three important observations are made: (1) dimer formation via D−D strand interactions as seen in the P32A structure and one of the subunit contacts in the H13F structure is improbable; (2) the CFG β-sheet is not part of the dimer interface; and (3) the ABED β-sheet is part of the dimer interface.

Considering the possibility of the D−D β-strand interaction in the dimer, we find that two of the residues expected to be buried by this interaction increase in reactivity as the dimer is formed. The interfaces formed by the interaction of D strands from two monomeric units as seen in the P32A dimer and one of the dimer units (AB chains) in H13F hexamer are shown in Figure 6. The two crystal structures show that the interaction surfaces of the antiparallel D strands span primarily the amino acids Glu50−Lys58. These interfaces predict reduced solvent accessibility of His51 on the D strand and Ser 57 and Lys58 on the DE loop. The calculated SASA of His51 decreases from 93 Å^2 in the monomeric protein (PDB ID: 2D4F) to 33 and 2 Å^2 in the P32A dimer and AB dimer in the H13F hexamer, respectively. Similarly, the SASA of Lys58 in the monomer decreases from 214 to ~167 Å^2 in the P32A and 88 Å^2 in the AB dimer. For Ser57, the SASA decreases from 58 Å^2 in the monomer to 0 Å^2 in the P32A dimer but increases slightly to 65 Å^2 in the AB dimer of the H13F hexamer. Hydrogen bonding likely occurs between the side chain of His51 and the backbone of Phe56 in the antiparallel D−D strand interaction of the AB chains of the H13F mutant (Figure 6B). In addition, in both the P32A and H13F crystal structures, Lys58 can form a salt bridge with Glu50 (Figure 6B). These interactions protect residues His51, Ser57, and Lys58 from solvent, and thus, if the dimer interface involves the D strands from two monomers, one would expect these residues to drop in reactivity as the dimer is formed. In our experiments, however, we find that His51, Lys58, and possibly Ser57 increase in reactivity as the dimer's concentration increases, suggesting that these interactions are not present in the wild-type dimer. From studies of the oligomerization properties of a series of β2m mutants in which the four His residues were replaced by different residues, Blaho and Miranker (*42*) recently speculated that His51 is an important residue at the interface of the tetramer and, therefore, not part of the dimer interface. Our results are consistent with this suggestion and provide additional evidence that His51 is not buried upon dimer formation.

The decreased reactivities of other residues provide further evidence against a dimer formed via the D−D strands and give support for a dimer involving the ABED β-sheet. The amino acids that exhibit a decrease in extent of modification upon dimer formation are shown in Figure 7A. All of these residues are located on the A, B, and E strands of β2m. Hence, the measured reactivity patterns are consistent with a dimer structure wherein the ABED sheet is part of the dimer interface. The decreased reactivity of these seven residues is consistent with both an antiparallel ABED−ABED arrangement as is formed by the B and C chains of the hexameric H13F mutant and a parallel ABED−ABED arrangement (Figure 8). Analysis of the BC dimer from the crystal structure of the hexameric H13F mutant reveals that all residues predicted to occur inside the dimer

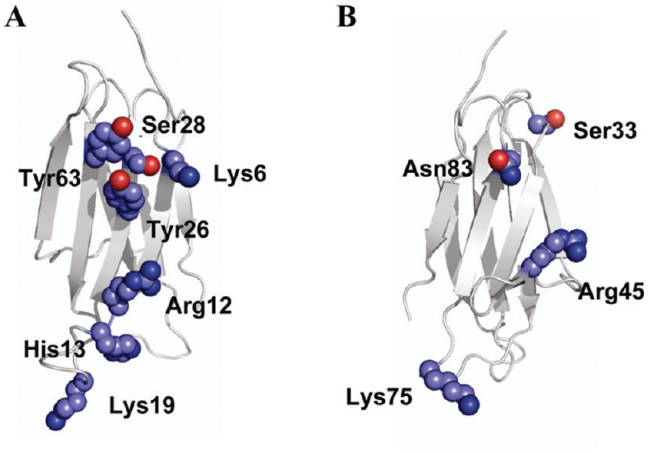

FIGURE 7: The probed amino acids that are located on the (A) ABED and (B) CFG sheets of β2m.

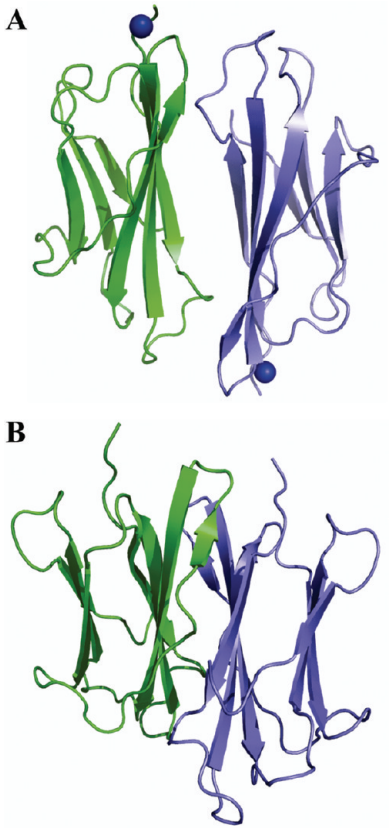

FIGURE 8: Two possible dimers formed via ABED−ABED intersheet interactions. (A) Antiparallel ABED−ABED arrangement as seen in the dimer formed by the B and C chains of the H13F mutant (PDB ID: 3CIQ). (B) Parallel ABED−ABED arrangement as calculated by the docking of two energy-minimized Cu-free β2m monomers obtained from the MHC complex (PDB ID: 1DUZ).

interface, Lys6 on the A strand, Arg12, His13, and Lys19 on the AB loop, Tyr26 and Ser28 on the B strand, and Tyr63 on the E strand, drop in reactivity after the onset of dimer formation. These data also correlate well with the decrease in calculated SASAs of most of these residues when comparing the monomeric structure to that of the BC dimer of the H13F mutant: Lys6, 199 to 0 Å^2; Arg12, 159 to 20 Å^2; Lys19, 316 to 90 Å^2; Tyr26, 73 to 0 Å^2; and Tyr63, 45 to 32 Å^2. The SASAs of His13 in the monomer and Phe13 in the BC dimer are 106 and 0 Å^2, respectively. For Ser28, the SASAs for monomeric β2m and the BC dimer are both 0 Å^2.

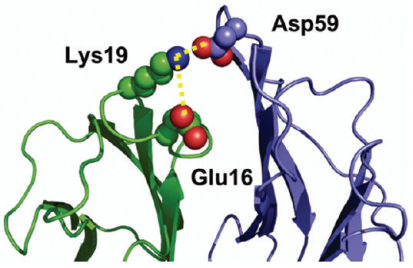

FIGURE 9: Interface between chains B and C in an antiparallel arrangement in the H13F hexamer (PDB ID: 3CIQ), showing the intersubunit salt bridges involving Asp59 and Lys19 and the complex salt bridge involving Glu16.

Many of these residues form new contacts in the BC chains of the H13F crystal structure that may help to stabilize the dimer. For example, Arg12 is very close to Tyr63, and the three-carbon chain of Arg's side chain probably forms a hydrophobic interaction with Tyr. Lys19 can form a salt bridge with Asp59 of another monomer in the antiparallel arrangement (Figure 9), which was recently postulated as one of the important interactions caused by Cu binding to monomeric β2m (*43*). Indeed, several structural and mutational analyses reveal a crucial role for electrostatic interactions in protein−protein interactions (*44*, *45*). In addition to experimental data, computational studies show that electrostatic interactions can substantially enhance the stability of protein−protein complexes (*46*, *47*). Lys19 is also in close proximity to Glu16, indicating that Lys19 might form a complex salt bridge with Glu16 of the same protein unit and Asp59 of another protein unit. Such networks involving two or more ion pairs are common at protein−protein interfaces and contribute more to protein stability than isolated ion pairs, which predominate in intramolecular interactions (*48*−*50*).

Detailed structural information is not available for a dimer with a parallel ABED−ABED interface, but we have used protein docking to test the viability of this potential dimer interface. Docking calculations involving two β2m monomers reveal that the dimer with the highest docking score has a parallel ABED−ABED interface with a crossing angle of ~35° (Figure 8B). Analysis of this docked dimer structure indicates that the residues that experimentally decrease in reactivity are also part of the dimer interface, with the exception of Lys19. The calculated SASAs for the residues in the docked dimer structure when compared to the monomeric crystal structure are as follows: Lys6, 199 to 19 Å^2; Arg12, 159 to 0 Å^2; His13, 106 to 32 Å^2; Lys19, 316 to 194 Å^2; Tyr26, 73 to 0 Å^2; Ser 28, 0 to 0 Å^2; and Tyr63, 45 to 0 Å^2. The decrease in SASA of Lys19 in the parallel dimer structure may be a consequence of forming a salt bridge with Glu16 of the same monomeric unit. Even though the drop in SASAs of most of these residues is consistent with the experimentally determined reactivities, close inspection of this docked dimer structure does not reveal any favorable salt bridge interactions between the two monomeric units. Indeed, calculations of the electrostatic component of the binding free energy indicate that the parallel arrangement has a slightly unfavorable electrostatic component. Because our previous work demonstrated the importance of salt bridges in dimer formation (*43*), we conclude that this parallel ABED−ABED interface is less likely than the antiparallel one.

The antiparallel ABED−ABED arrangement is also consistent with the measured surface area of the β2m dimer. The measured surface area of the monomer (6590 ± 140 Å^2)

compares well with the surface area (6500 Å^2) obtained from the monomeric crystal structure of β2m. The surface areas of the crystallographic dimer of the P32A dimer, the AB dimer of the H13F mutant, the BC dimer of the H13F mutant, and the parallel ABED−ABED arrangement from the docking calculations are 11988, 12093, 11524, and 11095 Å^2, respectively. The measured surface area for the dimer (11430 ± 150 Å^2) compares most favorably with the surface area of the antiparallel ABED−ABED arrangement as seen in the BC chains of the H13F mutant.

There are two other possible dimer forms with an ABED β-sheet interaction: (1) a parallel three-stranded (CFG) and four-stranded (ABED) interaction and (2) an antiparallel CFG-ABED interaction. Only four residues in the CFG sheet are probed by the covalent labels: His31, Arg45, Lys75, and Asn83 (Figure 7B). If the intersheet interaction involves the CFG sheet together with an ABED sheet, these four residues are expected to decrease in reactivity as the dimer forms. Our data clearly show, though, that the reactivity of Arg45 on the CD loop and Lys75 on EF loop increases upon dimer formation, indicating that these residues are more solvent accessible. There is no significant change in the reactivity of Asn83 on the F strand, suggesting that this residue is not part of the dimer interface. His31 on the BC loop had an initial drop in reactivity after the addition of Cu(II), but its reactivity remains constant during dimer formation. Hence, the reactivity pattern of these residues suggests that a dimer formed by the interaction of a CFG from one protein unit with an ABED sheet of another protein unit is unlikely.

Overall, our data support a β2m dimer interface that involves an antiparallel ABED−ABED interaction. As described above, the seven residues that are found at this interface all decrease in reactivity upon dimer formation. There are, however, seven other residues, Thr4, Arg45, His51, Ser57, Lys58, Lys75, and Lys94, that increase in reactivity as the dimer's concentration increases in solution. Are the reactivities of these residues consistent with the proposed dimer structure? The increased reactivity of five of these residues can be rationalized by comparing the monomeric structure and the crystal structure of the BC chains of the H13F hexamer. The increased reactivity of Arg45 might be explained by the breaking of a salt bridge interaction with Asp38 that is probably present in the monomer but not in the BC dimer of the H13F mutant. Arg45's SASA also increases slightly from 109 to 118 Å^2. Similarly, Lys94 probably forms a salt bridge with Glu77 in the monomer, but these two residues are much further apart in the BC dimer of the H13F mutant. The increased reactivities of His51, Lys58, and Lys75 correlate reasonably well with the increase in SASAs of these residues in the BC chains of the H13F mutant relative to the monomer: His51, 93 to 113 Å^2; Lys58, 214 to 327 Å^2; and Lys75, 245 to 302 Å^2.

SUMMARY AND CONCLUSIONS

In conclusion, our covalent labeling data indicate that the β2m dimer, which is formed prior to the β2m amyloid fibrils, has an interface that involves the antiparallel arrangement of ABED sheets from two monomers. Our confidence in this assignment comes from labeling data that cover almost one-half of the amino acids that are at the interface of the dimer and from comparison to the crystal structure of the hexameric H13F mutant, which appears to include many of the interactions present in the wild-type dimer. Our data clearly indicate that the dimer interface present in the P32A mutant of β2m is not the interface present in the wild-type dimer. Because β2m also forms tetramers and hexamers and not odd-ordered oligomers, the knowledge gained in this study about the dimer interface will serve as important foundational information for characterizing these larger oligomers. Information about these oligomeric intermediates should be useful for the development of therapeutics against DRA. More broadly speaking, covalent labeling along with MS detection appears to be a useful method for probing protein−protein interactions in situations where more than one protein species is present in solution. This ability could make this method useful for other amyloid-forming systems in which discrete oligomers precede fibril formation. For some amyloid-forming proteins, these small prefibrillar oligomers are thought to be responsible for cellular toxicity rather than the amyloid fibrils themselves (*51*, *52*), indicating the importance of studying their structures.

ACKNOWLEDGMENT

We thank Dr. Jonathan Wilson for help with the ETD experiments.

SUPPORTING INFORMATION AVAILABLE

(i) Plots showing the intensities of unmodified and modified forms of fragment Ile1−Tyr10 for three trials in the absence of Cu; (ii) tables presenting the intensities of unmodified and modified forms of peptide fragments containing residues Asn83, Lys94, and Lys6; (iii) plots illustrating the intensities of unmodified and modified forms of fragment Ile1−Tyr10 in the absence of Cu and 2 h after addition of Cu; (iv) plots illustrating the extent of NHSA modification of β2m residues throughout the course of the dimer formation reaction; (v) a figure showing the dose−response plot for two residues after reaction with DEPC; (vi) plots illustrating the extent of DEPC modification of residues throughout the course of the dimer formation reaction; (vii) tables presenting the intensities of unmodified and modified forms of peptide fragments containing residues Ser88, His51, and Tyr63; (viii) a figure showing the dose−response plot for β2m after reaction with BD; (ix) plots illustrating the extent of BD modification of Arg residues throughout the course of the dimer formation; and (x) a plot showing an ESI mass spectrum of β2m that was obtained after 5 days of incubation. This material is available free of charge via the Internet at http://pubs.acs.org.

REFERENCES

1. Floege, J., and Ehlerding, G. (1996) Beta-2-microglobulin associated amyloidosis. *Nephron 72*, 9–26.
2. Ayers, D. C., Athanasou, N. A., Woods, C. G., and Duthie, R. B. (1993) Dialysis arthropathy of the hip. *Clin. Orthop. Relat. Res. 290*, 216–224.
3. Menaa, C., Esser, E., and Sprague, S. M. (2008) β2-microglobulin stimulates osteoclast formation. *Kidney Int. 73*, 1275–1281.
4. Keating, M. J. (1999) Chronic lymphocytic leukemia. *Semin. Oncol. 26*, 107–114.
5. Malaguarnera, M., Restuccia, S., Di Fazio, I., Zoccolo, A. M., Trovato, B. A., and Pistone, G. (1997) Serum beta-2-microglobulin in chronic hepatitis C. *Dig. Dis. Sci. 42*, 762–766.
6. McParland, V. J., Kad, N. M., Kalverda, A. P., Brown, A., Kirwin-Jones, P., Hunter, M. G., Sunde, M., and Radford, S. E. (2000) Partially unfolded states of β_2-microglobulin and amyloid formation *in vitro*. *Biochemistry 39*, 8735–8746.
7. Esposito, G., Michelutti, R., Verdone, G., Viglino, P., Hernandez, H., Robinson, C. V., Amoresano, A., Dal Piaz, F., Monti, M., Pucci, P., Mangione, P., Stoppini, M., Merlini, G., Ferri, G., and Bellotti, V. (2000) Removal of the N-terminal hexapeptide from human β_2-microglobulin facilitates protein aggregation and fibril formation. *Protein Sci. 9*, 831–845.

8. Relini, A., Canale, C., De Stefano, S., Rolandi, R., Giorgetti, S., Stoppini, M., Rossi, A., Fogolari, F., Corazza, A., Esposito, G., Gliozzi, A., and Belloti, V. (2006) Collagen plays an active role in the aggregation of β_2-microglobulin under physiopathological conditions of dialysis-related amyloidosis. *J. Biol. Chem. 281*, 16521–16529.
9. Ohhashi, Y., Kihara, M., Naiki, H., and Goto, Y. (2005) Ultrasonication-induced amyloid fibril formation of β_2-microglobulin. *J. Biol. Chem. 280*, 32843–32848.
10. Morgan, C. J., Gelfans, M., Atreya, C., and Miranker, A. D. (2001) Kidney dialysis-associated amyloidosis: a molecular role for copper in fiber formation. *J. Mol. Biol. 309*, 339–345.
11. Villanueva, J., Hoshino, M., Katou, H., Kardos, J., Hasegawa, K., Naiki, H., and Goto, Y. (2004) Increase in the conformational flexibility of β_2-microglobulin upon copper binding: a possible role for copper in dialysis-related amyloidosis. *Protein Sci. 13*, 797–809.
12. Bush, A. I., and Tanzi, R. E. (2002) The galvanization of β-amyloid in Alzheimer's disease. *Proc. Natl. Acad. Sci. U.S.A. 99*, 7317–7319.
13. Uversky, V. N., Li, J., and Fink, A. L. (2001) Metal-triggered structural transformations, aggregation, and fibrillation of human α-synuclein. A possible molecular link between Parkinson's disease and heavy metal exposure. *J. Biol. Chem. 276*, 44284–44296.
14. Jobling, M. F., Huang, X., Stewart, L. R., Barnham, K. J., Curtain, C., Volitakis, I., Perugini, M., White, A. R., Cherny, R., A., Masters, C. L., Barrow, C. J., Collins, S. J., Bush, A. I., and Cappai, R. (2001) Copper and zinc binding modulates the aggregation and neurotoxic properties of the prion peptide PrP106-126. *Biochemistry 40*, 8073–8084.
15. Wadsworth, J. D., Hill, A. F., Joiner, S., Jackson, G. S., Clarke, A. R., and Collinge, J. (1999) Strain-specific prion-protein conformation determined by metal ions. *Nat. Cell Biol. 1*, 55–59.
16. Davis, D. P., Gallo, G., Vogen, S. M., Dul, J. L., Sciarretta, K. L., Kumar, A., Raffen, R., Stevens, F. J., and Argon, Y. (2001) Both the environment and somatic mutations govern the aggregation pathway of pathogenic immunoglobulin light chain. *J. Mol. Biol. 313*, 1021–1034.
17. Antwi, K., Mahar, M., Srikanth, R., Olbris, M. R., Tyson, J. F., and Vachet, R. W. (2008) Cu(II) organizes beta-2-microglobulin oligomers but is released upon amyloid formation. *Protein Sci. 17*, 748–759.
18. Calabrese, M. F., and Miranker, A. D. (2007) Formation of a stable oligomer of β-2-microglobulin requires only a transient encounter with Cu(II). *J. Mol. Biol. 367*, 1–7.
19. Eakin, C. M., Berman, A. J., and Miranker, A. D. (2006) A native to amyloidogenic transition regulated by a backbone trigger. *Nat. Struct. Mol. Biol. 13*, 202–208.
20. Calabrese, M. F., Eakin, C. M., Wang, J. M., and Miranker, A. D. (2008) A regulatable switch mediates self-association in an immunoglobulin fold. *Nat. Struct. Mol. Biol. 15*, 965–971.
21. Mendoza, V. L., and Vachet, R. W. (2009) Probing protein structure by amino acid-specific covalent labeling and mass spectrometry. *Mass Spec. Rev. 28*, 785–815.
22. Fliss, H., and Viswanatha, T. (1979) 2,3-Butanedione as a photosensitizing agent—Application to alpha-amino acids and alpha-chymotrypsin. *Can. J. Biochem. 57*, 1267–1272.
23. Riordan, J. F. (1979) Arginyl residues and anion binding sites in proteins. *Mol. Cell. Biochem. 26*, 71–92.
24. Kaltashov, I. A., and Mohimen, A. (2005) Estimates of protein surface areas in solution by electrospray ionization mass spectrometry. *Anal. Chem. 77*, 5370–5379.
25. Kihara, M., Chatani, E., Iwata, K., Yamamoto, K., Matsuura, T., Nakagawa, A., Naiki, H., and Goto, Y. (2006) Conformation of amyloid fibrils of β2-microglobulin probed by tryptophan mutagenesis. *J. Biol. Chem. 281*, 31061–31069.
26. Fraczkiewicz, R., and Braun, W. (1998) Exact and efficient analytical calculation of the accessible surface areas and their gradients for macromolecules. *J. Comput. Chem. 19*, 319–333.
27. Khan, A. R., Baker, B. M., Ghosh, P., Biddison, W. E., and Wiley, D. C. (2000) The structure and stability of an HLA-A*0201/octameric tax peptide complex with an empty conserved peptide-N-terminal binding site. *J. Immunol. 164*, 6398–6405.
28. Verdone, G., Corazza, A., Viglino, P., Pettirossi, F., Giorgetti, S., Mangione, P., Andreola, A., Stoppini, M., Bellotti, V., and Esposito, G. (2002) The solution structure of human β2-microglobulin reveals the prodromes of its amyloid transition. *Protein Sci. 11*, 487–499.
29. Mahoney, M., and Jorgensen, A. (2000) A five-site model for liquid water and the reproduction of the density anomaly by rigid, nonpolarizable potential functions. *J. Chem. Phys. 112*, 8911–8922.
30. Cornell, W., Cieplak, P., Bayly, C., Gould, I., Merz, K., Ferguson, D., Spellmeyer, D., Fox, T., Caldwell, J., and Kollma, P. (1995) A second generation force field for the simulation of proteins, nucleic acids, and organic molecules. *J. Am. Chem. Soc. 117*, 5179–5197.
31. Sorin, E. J., and Pande, V. S. (2005) Exploring the helix-coil transition via all-atom equilibrium ensemble simulations. *Biophys. J. 88*, 2472–2493.
32. van der Spoel, D., Lindahl, E., Hess, B., Groenhof, G., Mark, A., and Berendsen, H. (2005) Gromacs: fast, flexible, and free. *J. Comput. Chem. 26*, 1701–1719.
33. Lindahl, E., Hess, B., and van der Spoel, D. (2001) Gromacs 3.0: a package for molecular simulation and trajectory analysis. *J. Mol. Mod. 7*, 306–317.
34. Berendsen, H., van der Spoel, D., and van Drunen, R. (1995) Gromacs: a message-passing parallel molecular dynamics implementation. *Comput. Phys. Commun. 91*, 43–56.
35. Chen, T., Li, L., and Weng, Z. (2002) Docking unbound proteins using shape complementary, desolvation, and electrostatics. *Proteins 47*, 281–294.
36. Chen, T., and Weng, Z. (2003) ZDOCK: an initial-stage protein-docking algorithm. *Proteins 52*, 80–87.
37. Holst, M. J., Baker, N. A., and Wang, F. (2000) Adaptive multilevel finite element solution of the Poisson-Boltzmann equation. I. Algorithms and examples. *J. Comput. Chem. 21*, 1319–1242.
38. Mendoza, V. L., and Vachet, R. W. (2008) Protein surface mapping using diethylpyrocarbonate with mass spectrometric detection. *Anal. Chem. 80*, 2895–2904.
39. Hassani, O., Mansuelle, P., Cestele, S., Bourdeaux, M., Rochat, H., and Sampieri, F. (1999) Role of lysine and tryptophan residues in the biological activity of toxin VII (Tsγ) from the scorpion *Tityus serrulatus*. *Eur. J. Biochem. 260*, 76–86.
40. Okon, M., Bray, P., and Vucelic, D. (1992) ^{1}H-NMR assignments and secondary structure of human beta-2-microglobulin in solution. *Biochemistry 31*, 8906–8915.
41. Eakin, C. M., Attenello, F. J., Morgan, C. J., and Miranker, A. D. (2004) Oligomeric assembly of native-like precursors precedes amyloid formation by β-2-microglobulin. *Biochemistry 43*, 7808–7815.
42. Blaho, D. V., and Miranker, A. D. (2009) Delineating the conformational elements responsible for Cu^{2+}-induced oligomerization of beta-2 microglobulin. *Biochemistry 48*, 6610–6617.
43. Srikanth, R., Mendoza, V. L., Bridgewater, J. D., Zhang, G., and Vachet, R. W. (2009) Copper binding to β-2-microglobulin and its pre-amyloid oligomers. *Biochemistry 48*, 9871–9881.
44. Sheinerman, F. B., Norel, R., and Honig, B. (2000) Electrostatic aspects of protein-protein interactions. *Curr. Opin. Struct. Biol. 10*, 153–159.
45. Keskin, O., Gursov, A., Ma, B., and Nussinov, R. (2008) Principles of protein-protein interactions: what are the preferred ways for proteins to interact? *Chem. Rev. 108*, 1225–1244.
46. Kundrotas, P. J., and Alexov, E. (2006) Electrostatic properties of protein-protein complexes. *Biophys. J. 91*, 1724–1736.
47. Dong, F., and Zhou, H.-X. (2006) Electrostatic contribution to the binding stability of protein−protein complexes. *Proteins 65*, 87–102.
48. Musafia, B., Buchner, V., and Arad, D. (1995) Complex salt bridges in proteins: statistical analysis of structure and function. *J. Mol. Biol. 254*, 761–770.
49. Risal, D., Gourinath, S., Himmel, D. M., Szent-Gyorgyi, A. G., and Cohen, C. (2004) Myosin subfragment 1 structures reveal a partially bound nucleotide and a complex salt bridge that helps couple nucleotide and actin binding. *Proc. Natl. Acad. Sci. U.S.A. 101*, 8930–8935.
50. Xu, G. Z., Liu, R. T., Zak, O., Aisen, P., and Chance, M. R. (2005) Structural allostery and binding of the transferrin·receptor complex. *Mol. Cell. Proteomics 4*, 1959–1967.
51. Bucciantini, M., Giannoni, E., Fabrizio, C., Baroni, F., Formigli, L., Zurdo, J., Taddei, N., Ramponi, G., Dobson, C. M., and Stefani, M. (2002) Inherent toxicity of aggregates implies a common mechanism for protein misfolding diseases. *Nature 416*, 507–511.
52. Mendes Sousa, M., Cardoso, I., Fernandes, R., Guimaraes, A., and Saraiva, M. J. (2001) Deposition of transthyretin in early stages of familial amyloidotic polyneuropathy. Evidence for toxicity of nonfibrillar aggregates. *Am. J. Pathol. 159*, 1993–2000.